Synthesis of First-Row Transition Metal Catalysts for Alkene Hydroamination

Emily Dagasso
T00609571

CHEM 4480: Directed Studies in Chemistry

Supervisor: Dr. Dipesh Prema | Co-supervisor: Dr. Kingsley Donkor

Submitted: April 14, 2023

Abstract

Amines are a versatile group of organic compounds that have a wide range of applications in multiple industries, including pharmaceuticals and agriculture. Various methods are utilized in the synthesis of amines, however, catalytic hydroamination is favored due to its high atom economy. Within large-scale industries, hydroamination reactions are commonly catalyzed by rare transition metals – options that are expensive, toxic and have a low abundance. This project focuses on the development of catalysts utilizing inexpensive and readily available first-row transition metals. Bulky imino-phosphine ligands were first synthesized via a Schiff base condensation reaction of 2-(diphenylphosphino)benzaldehyde and either 2,4,6-triphenylaniline or 4-tritylaniline. The synthesized 4-tritlyaniline imino-phosphine ligand was then coordinated to two first-row transition metals, zinc chloride and cobalt(II) chloride. The products were characterized utilizing a variety of spectroscopic techniques, including ^{1}H, ^{13}C, ^{31}P NMR and IR spectroscopy, and apart from the cobalt complex, all products confirmed imine formation and successful complexation. This research introduces the synthesis of a novel hydroamination catalyst, comprised of abundant, inexpensive, and non-toxic materials, that has the potential to be utilized as a sustainable industrial alternative.

Introduction

Nitrogen containing compounds are building blocks in inorganic chemistry and represent a vital component to countless industries, with applications ranging from simple dyes to cleaning supplies. On account of the increased global demand for amine-based products, these commodity chemicals are projected to grow annually by 8.3 %, a staggering statistic indicating their world-wide significance.[1] A direct result of their rising market value is the need for an inexpensive and efficient chemical synthesis that can be implemented at the industrial level. Available methods for alkyl amine synthesis include allylic and reductive amination as well as an array of hydrofunctionalization reactions including hydroaminomethylation, hydrocyanation and hydrogenation.[1] However, these reactions are known to utilize hazardous chemicals, such as cyanide, and generate waste and by-products.[1] In contrast, the hydroamination reaction, shown in Figure. 1, is a very attractive route to nitrogen containing compounds due to its simplicity and proposed 100 % atom efficiency.[1,2,3,4,5] The qualities of the hydroamination reaction are well sought after by industry especially with the movement toward greener chemistry, a world-wide initiative that aims to reduce or eliminate the use or generation of chemical pollution.[6]

Figure. 1 Hydroamination of substituted alkene with an amine utilizing a metal complex catalyst yielding a Markovnikov or anti-Markovnikov product.

Hydroamination is a chemical reaction that involves the direct addition of an N-H bond, oftentimes an alkyl amine, to an unsaturated C-C- bond, being alkenes or alkynes, which allows the formation of amines, such as enamines and imines.[2] Of the available functional groups able to participate within this reaction, alkynes have achieved the most success due to its increased spontaneity compared to alkenes.[2,5] Although research has focused on the use of non-activated alkenes within hydroamination reactions due to their ability to directly product stable amines.[4] This process remains challenging as alkenes have significantly higher reaction barriers and

increased electron density between the carbon bonds.[1,3,7] As a result, an effort to develop effective catalysts has been the focus of much hydroamination research in recent years.

Catalytic approaches to hydroamination reactions have been reported in past decades to further increase its efficiency for industrial applications. These catalysts commonly involve precious metals, with studies including elements such as mercury, thallium[2], rhodium, palladium, and zirconium[8], as well as rare-earth metals such as organolanthanides[9]. Despite these catalysts characteristic efficiency, stability, and selectivity, precious metals and rare-earth metals are heavy, non-abundant, expensive, as well as hazardous to the environment due to their associated toxicity.[7] In light of the climate crisis, efforts are focused on developing catalysts utilizing first-row transition metals, including scandium, titanium, vanadium, chromium, manganese, iron, cobalt, nickel, copper and zinc. Notably, these elements are considerably more abundant within the earth's crust as well as less toxic to the environment than the current metals within hydroamination catalysts. Synthetic and computational research in recent decades have indicated that it is not only possible to utilize elements such as copper,[10,11] iron[12] and nickel[13] as catalysts within the hydroamination of alkenes, but that they are also efficient and effective systems.

Alkene catalytic hydroamination generates two distinct products as a result of complications surrounding site selectivity. As demonstrated in Figure. 1, the process can produce a Markovnikov product, where the amine is added to the most substituted carbon, or oppositely an anti-Markovnikov product, where the amine is added to the least substituted carbon. The final product is dependent on the interactions of both the catalyst system as well as the substrates involved within the reaction.[14] Most hydroamination studies report preferential Markovnikov selectivity, indicating that anti-Markovnikov addition is a more challenging endeavour.[15,16] However, due to the linearity of anti-Markovnikov products and therefor wide applicability to industrial applications, these products are more sought after in academia and industry.[1]

Further, the hydroamination process is catalyzed through two separate mechanisms, initial activation of the alkene or amine, as demonstrated in Figure. 2.[13] Alkene activation occurs through various pathways, including alkene π-coordination to a Lewis acidic metal center, hydrometallation, or hydrogen atom transfer.[17] The most common alkene activation mechanism in literature is reported to be by π-coordination, where the metal is coordinated to the alkene, followed by the nucleophilic attack of the amine. However, activation of the alkene in the presence of amines is known to be difficult, as the amines would rather displace than attack the coordinated alkene due to amines being strong ligands for transition metal centres.[3] Alternatively, amine

activation ensues through either deprotonation of the amine by a basic catalyst, or oxidative addition of the amine to the metal centre. The latter process is through to be a more efficient method of amine activation and is demonstrated by inserting the transition metal complexes into unreactive nitrogen-hydrogen, N-H, bonds.[18] A review conducted by Colonna et al. indicates that alkene hydroamination is more efficient through amine protonation pathways than the alternative alkene activation when considering first-row transition metals, such as iron, cobalt, copper and zinc.[17]

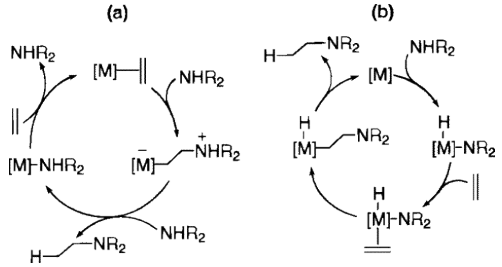

Figure. 2 Mechanistic pathways for hydroamination reactions catalyzed by a metal [M] complex. (a) Activation of the alkene (b) Activation of the amine.[13]

Herein, this research reports the synthesis and characterization of two distinct imino-phosphine ligands coordinated to readily abundant first-row transition metals. The imino-phosphine ligands were synthesized through a simple Schiff base condensation reaction, involving a primary amine and an aldehyde, as shown in Figure. 3. Imino-phosphines were chosen to be the ligand within this study due to their uniquely bulky and bidentate structure. Amines, when introduced to metal complexes, are known to strongly bind to the coordination sides of the metals through their electron lone pair, which can ultimately prevent coordination of the alkene and N-H bond activation.[1,19] Therefore, it is theorized that the characteristic shape of the imino-phosphine ligands will inhibit the amine complexation through steric hindrance and guide the included metal toward N-H bond insertion.

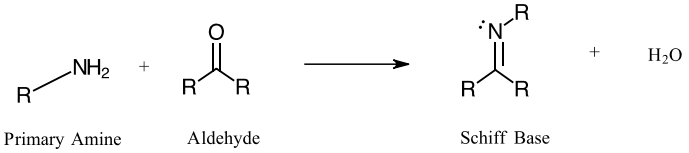

Figure. 3 Reaction mechanism for Schiff base condensation.

Experimental

Instrumentation

^{1}H, ^{13}C and ^{31}P spectra were recorded on the Bruker Avance 500 MHz NMR spectrometer. FT-IR spectrum was obtained from the Perkin Elmer FT-IR spectrometer. Both spectrometers were provided by Thompson Rivers University

Synthesis of the 2,4,6-Triphenyllaniline Imino-phosphine Ligand

The synthesis of the 2,4,6-triphenylaniline imino-phosphine ligand is reported in Scheme. 1, with reaction conditions and yield reported in Table. 1. This ligand was prepared twice, once in a small-scale batch and once in a large-scale batch. The initial batch resulted in a mass of 0.04967 g and final yield of 58.0 %, whereas the large-scale bath resulted in a yield of 0.09638 g and 70.1%.

The reflux apparatus was prepared in the fumehood as per Figure. 3. The following reagents were added directly into a 25 mL round-bottom flask, RBF, utilizing an analytical balance: 2-(diphenylphosphino) benzaldehyde (2-DPPB), 2,4,6-triphenylaniline (2,4,6-TPA), 2,4,6-trimethylbenzoic acid (2,4,6-TMBA) and calcium chloride. Then, 7 mL of tetrahydrofuron (THF) solvent was added to the 25-mL RBF followed by a small stir bar. Once all solids were dissolved in the solvent, the solution appeared to be clear with a light-yellow colour. The RBF was then attached to the previously prepared reflux apparatus and placed in an oil bath. The solution was then set to stir with medium intensity on low heat.

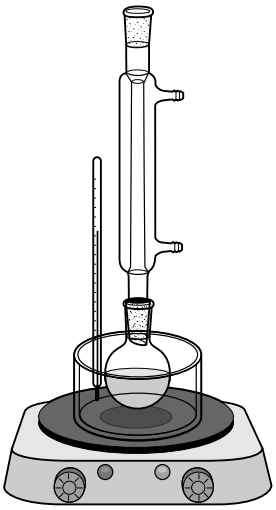

Figure. 4 Reflux apparatus set-up

The solution was refluxed for 2.5 hours, with the temperature remaining between 69-75 ℃. Once the reflux was complete, the solution was taken off from the apparatus and allowed to cool to room temperature. The contents of the RBF were then vacuum filtered with a fritted glass funnel, and the yellow filtrate was collected. The filtrate was then placed into a clean 25 mL RBF prior to parafilming and placing in the fridge for either 4 (large-scale) or 7 (small-scale) days.

After retrieving from the fridge, the solution was a clear yellow with no apparent precipitate. The solution was then placed on the rotary evaporator to remove the THF. Following removing the solvent, the contents of the RBF was a viscous dark yellow substance. The solution was the recrystallized by placing into a warm water bath and adding 2 mL of methanol dropwise

whilst periodically stirring. Once white precipitate became apparent, the solution was cooled to room temperature prior to the bottom of the RBF being scratched. The RBF was then parafilmed and put in the fridge.

The solution was left in the fridge for 3 (large-scale) or 7 (small-scale) days prior to being retrieved. Once retrieved, the solution was bright yellow with white crystals near the bottom of the flask. The solution was then vacuum filtered with a fritted glass funnel, and the solid yellow precipitate was collected, weighed, and stored.

Synthesis of the 4-Tritylaniline Imino-phosphine Ligand

The synthesis of the 4-tritulaniline imino-phosphine ligand is reported in Scheme. 2, with reaction conditions and yield reported in Table. 2. Several recrystallization solvents were tested for optimization of the 4-tritylaniline imino-phosphine ligand product, including independent or combination amounts of methanol, tetrahydrofuran, ethanol, chloroform and dichloromethane. The results of the recrystallization solvent tests can be found in Table. 3. The resulting mass of this synthesis was 0.64549 g, with a yield of 97.1 %.

The reflux apparatus was prepared in the fumehood as per Figure. 3. The following reagents were added directly into a 50 mL round-bottom flask, RBF, utilizing an analytical balance: 0.3408 g 2-(diphenylphosphino)benzaldehyde (2-DPPB), 0.3762 g 4-tritylaniline, 0.1991 g 2,4,6-trimethylbenzoic acid (2,4,6-TMBA) and 0.3746 g calcium chloride ($CaCl_2$). Then, 10 mL of tetrahydrofuron (THF) solvent was added to the 50-mL RBF followed by a small stir bar. Once all solids were dissolved in the solvent, the solution appeared to be clear with a light-yellow colour. The RBF was then attached to the previously prepared reflux apparatus and placed in an oil bath. The solution was then set to stir with medium intensity on low heat.

The solution was refluxed for 3.5 hours, with the temperature remaining between 60-70 °C. Once the reflux was complete, the solution was taken off from the apparatus and allowed to cool to room temperature. The solution had a cloudy light-yellow appearance. The RBF was then parafilmed and put in the fridge.

After retrieving from the fridge, the solution was a cloudy light-yellow. The solution was then placed on the rotary evaporator to remove the THF. Following removing the solvent, the contents of the RBF was a viscous yellow substance. The solution was the recrystallized by placing into a warm water bath and adding 3 mL of both dichloromethane (DCM) and methanol dropwise whilst periodically stirring. Following the recrystallization there was solid white precipitate

attached to the sides of the RBF with a cloudy yellow liquid in the middle. The solution was then vacuum filtered with a fritted glass funnel, with the white precipitate being collected, weighed and stored.

Coordination of the 4-Tritylaniline Imino-phosphine Ligand to Cobalt (II) Chloride

The coordination of 4-tritylaniline imino-phosphine ligand a first-row transition metals, cobalt, is reported in Scheme. 3. Reaction conditions and yields are reported in Table. 4. The resulting yield of this complexation reaction was 0.11059 g, and 99.5 %.

Cobalt (II) chloride was measured on an analytical balance and added directly to a 25 mL RBF. A small stir bar was added to the solution along with 2.5 mL of diethyl ether. The solution was then heated on low heat whilst stirring to dissolve the metal solid. Once completely dissolved the mixture was cloudy with a light purple hue. Approximately 0.01 g of the previously synthesized 4-tritylaniline ligand was measured on an analytical balance and added directly to the metal solution. Immediately the solution turned a dark green colour. The mixture was placed on low heat with stirring for 2 hours before a small amount of precipitate was eident on the bottom of the RBF. The solution was cooled to room temperature, parafilmed and placed within the fridge.

The mixture was retrieved from the fridge a day later where it was evident crystallization occurred due to the large chunks of precipitate on the bottom of the RBF. The solution was vacuum filtered with a fritted glass funnel, and a light blue powder was weighed and stored.

Coordination of the 4-Tritylaniline Imino-phosphine Ligand to Zinc Chloride

The coordination of the 4-tritylaniline imino-phosphine ligand a first-row transition metals, cobalt, is reported in Scheme. 4. Reaction conditions and yields are reported in Table. 4. The resulting yield of this complexation reaction was 0.06493 g and 58.4 %.

Zinc chloride was measured on an analytical balance and added directly to a 25 mL RBF. A small stir bar was added to the solution along with 2.5 mL of diethyl ether. The solution was then heated on low heat whilst stirring to dissolve the metal solid. Once completely dissolved the mixture was cloudy with a pale-yellow hue. Approximately 0.01 g of the previously synthesized 4-tritylaniline ligand was measured on an analytical balance and added directly to the metal solution, where no significant changes of colour occurred. The mixture was placed on low heat with stirring for 2 hours before a small amount of precipitate was eident on the bottom of the RBF. The solution was cooled to room temperature, parafilmed and placed within the fridge.

The mixture was retrieved from the fridge a day later where it was evident crystallization occurred due to the chunks of precipitate on the bottom of the RBF. The solution was vacuum filtered with a fritted glass funnel, and a pale-yellow powder was weighed and stored.

Results

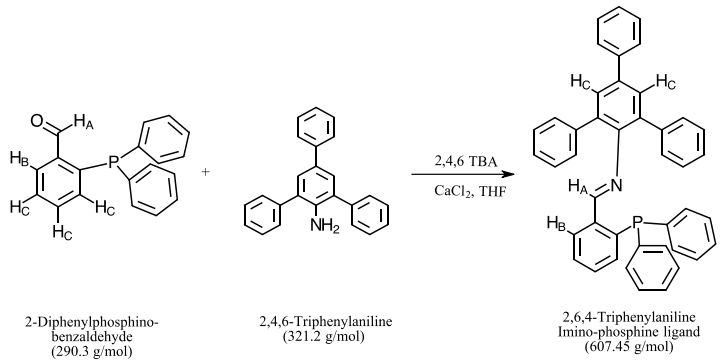

Scheme. 1 Reaction mechanism of the 2,4,6-triphenylaniline imino-phosphine ligand with hydrogens labelled for NMR analysis.

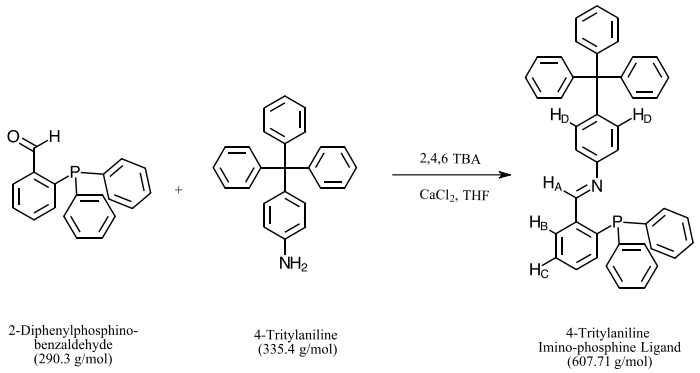

Scheme. 2 Reaction mechanism of the 4-tritylaniline imino-phosphine ligand with hydrogens labelled for NMR analysis.

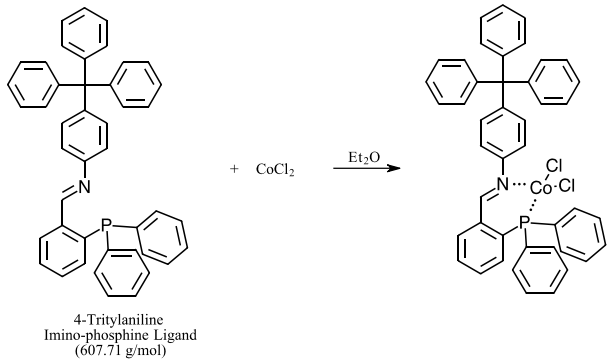

Scheme. 3 Coordination of the 4-tritylaniline imino-phosphine ligand to cobalt (II) chloride.

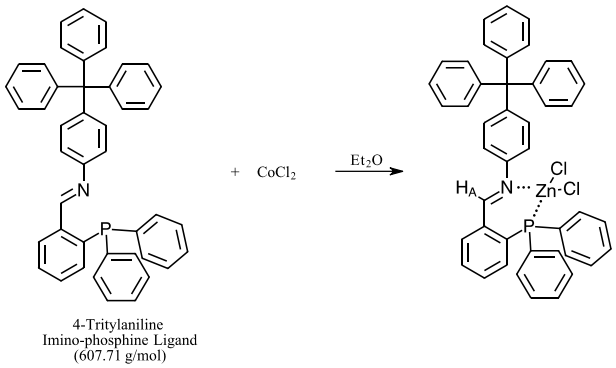

Scheme. 4 Coordination of the 4-tritylaniline imino-phosphine ligand to $ZnCl_2$ with hydrogens labelled for NMR analysis.

Table. 1 Reaction conditions of the 2,4,6-triphenylaniline imino-phosphine ligand

Scale	2-DPPB (g)	2,4,6-TPA (g)	2,4,6-TMBA (g)	$CaCl_2$ (g)	Reflux Time (h)	Yield (g)	Percent Yield
Small Scale	0.04069	0.047359	0.47881	0.06531	3.0	0.04976	58.0 %
Large Scale	0.06572	0.07768	0.1208	0.0738	2.5	0.09638	70.1 %

Table. 2 Reaction conditions of the 4-tritylaniline imino-phosphine ligand

2-DPPB (g)	4-tritylaniline (g)	2,4,6-TMBA (g)	$CaCl_2$ (g)	Yield (g)	Reflux Time (h)	Percent Yield
0.3408	0.3762	0.1991	0.3746	0.64549	3.5	97.1 %

Table. 3 Solubility tests for recrystallization of the 4-tritylaniline imino-phosphine ligand

Solvent Utilized	Dissolution of Precipitate	Appearance of Crystals
Methanol	Precipitate did not dissolve	No
Methanol + Tetrahydrofuran	Precipitate dissolved slightly	No
Ethanol	Precipitate dissolved slightly	No
Chloroform	Precipitate dissolved completely	No
Dichloromethane	Precipitate dissolved completely	No
Dichloromethane + Methanol	Precipitate dissolved completely	Yes

Table. 4 Reaction conditions of the 4-tritylaniline imino-phosphine ligand coordinated to $CoCl_2$ and $ZnCl_2$.

Metal	4-Tritylaniline imino-phosphine ligand (g)	Metal (g)	Solvent	Reflux Time (h)	Yield (g)	Percent Yield
$CoCl_2$	0.10	0.10	Ethyl Ether	1.5	0.11059	99.5 %
$ZnCl_2$	0.10	0.10	Ethyl Ether	1.5	0.06493	58.4 %

Table. 5 ^{1}H NMR data for 2-dipheylphosphinobenzaldehyde in $CDCl_3$

δ(ppm)	Multiplicity	Integration	Assignment
10.5137	Singlet	1.0	**H**-C=O (H_A)
7.9793	D of D	1.0	H_B
7.5 – 7.4	Multiplet	3.0	H_C
7.2600	Singlet	1.0	$CDCl_3$
7.2 – 6.9	Multiplet	14.0	Aromatic Hydrogens
1.6041	Singlet	~	Water Impurity

Table. 6 ^{1}H NMR data for the 2,4,6-triphenylaniline imino-phosphine ligand in $CDCl_3$ (large scale)

δ(ppm)	Multiplicity	Integration	Assignment
10.5340	Singlet	~	Starting Material
8.9566	Doublet	1.0	**H**-C=N (H_A)
7.9276	D of D	1.0	H_B
7.6857	Doublet	2.0	H_C
7.6238	Singlet	2.0	Aromatic Hydrogens
7.6 – 7.2	Multiplet	24.0	Aromatic Hydrogens
7.26	Singlet	1.0	$CDCl_3$
7.2 – 7.0	Multiplet	7.0	Aromatic Hydrogens
6.900	Multiplet	1.0	Aromatic Hydrogens
3.7726	Singlet	~	Residual THF
3.5126	Singlet	~	Residual Methanol
1.5714	Singlet	~	Water Impurity

Table. 7 ^{1}H NMR data for the 4-tritylaniline imino-phosphine ligand in $CDCl_3$

δ(ppm)	**Multiplicity**	**Integration**	**Assignment**
9.1616	Doublet	1.0	**H**-C=N (H_A)
8.2244	D of D	1.0	H_B
7.4904	Triplet	1.0	H_C
7.4 – 7.1	Multiplet	33.0	Aromatic Hydrogens
7.2601	Singlet	1.0	$CDCl_3$
6.9769	Multiplet	1.0	Aromatic Hydrogens
6.9026	Doublet	2.0	H_D
5.3000	Singlet	~	Residual DCM
3.7886	Multiplet	~	Residual THF

Table. 8 ^{1}H NMR data for the 4-tritylaniline imino-phosphine ligand coordinated to zinc chloride in $CDCl_3$

δ(ppm)	**Multiplicity**	**Integration**	**Assignment**
8.4229	Singlet	1.0	**H**-C=N (H_A)
7.8 – 7.7	Multiplet	3.0	Aromatic Hydrogens
7.75 – 7.55	Multiplet	9.0	Aromatic Hydrogens
7.55 – 7.45	Multiplet	5.0	Aromatic Hydrogens
7.3 – 7.1	Multiplet	27.0	Aromatic Hydrogens
77.2600	Singlet	1.0	$CDCl_3$

Table. 9 ^{1}H NMR with ^{31}P decoupled data for the 2,4,6-triphenylaniline imino-phosphine ligand

δ(ppm)	**Multiplicity**	**Integration**	**Assignment**
10.5595	Singlet	~	Starting Material
8.9607	Singlet	1.0	**H**-C=N (H_A)
7.9589	Doublet	1.0	H_B
7.7104	Doublet	2.0	H_C
7.6532	Singlet	1.0	Aromatic Hydrogens
7.6 – 7.0	Multiplet	44.0	Aromatic Hydrogens
6.9158	Doublet	2.0	Aromatic Hydrogens
3.7994	Multiplet	~	Residual THF

Table. 10 ^{1}H NMR with ^{31}P decoupled data for the 4-tritylaniline imino-phosphine ligand

δ(ppm)	**Multiplicity**	**Integration**	**Assignment**
9.1546	Singlet	1.0	**H**-C=N (H_A)
8.2178	D of D	1.0	H_B
7.4831	Triplet	1.0	H_C
7.4 – 7.1	Multiplet	33.0	Aromatic Hydrogens
6.9694	Doublet	1.0	Aromatic Hydrogens
6.8955	Doublet	2.0	H_D
5.3235	Singlet	~	Residual DCM
3.7891	Multiplet	~	Residual THF

Table. 11 ^{13}C NMR data for the 2,4,6-triphenylaniline imino-phosphine ligand in $CDCl_3$

δ(ppm)	**Assignment**
163.9418	**C**=N
150 – 125	Aromatic Carbons
77.0463	$CDCl_3$

Table. 12 ^{13}C NMR data for the 4-tritylaniline imino-phosphine ligand in $CDCl_3$

δ(ppm)	**Assignment**
158.5061	**C**=N
150 – 120	Aromatic Carbons
77.0643	$CDCl_3$

Table. 13 ^{31}P NMR data for 2-dipheylphosphinobenzaldehyde in $CDCl_3$

δ(ppm)	**Assignment**
-11.6314	Ph-P-Ph

Table. 14 ^{31}P NMR data for the 2,4,6-triphenylaniline imino-phosphine ligand in $CDCl_3$

δ(ppm)	**Assignment**
-11.6297	Starting Material (2-DPPB)
-18.8986	Ph-P-Ph

Table. 15 ^{31}P NMR data for the 4-tritylaniline imino-phosphine ligand in $CDCl_3$

δ(ppm)	**Assignment**
-13.6776	Ph-P-Ph

Table. 16 FT-IR data for the 2,4,6-triphenylaniline imino-phosphine ligand

Band Positions (± 4 cm^{-1})	**Relative Intensities**	**Functional Group**
1633.78	Medium	C=N

Table. 17 FT-IR data for the 4-tritylaniline imino-phosphine ligand

Band Positions (± 4 cm^{-1})	**Relative Intensities**	**Functional Group**
1615.24	Weak	C=N

Discussion

This project focused on the development of a hydroamination catalyst utilizing imino-phosphine ligands and readily available first-row transition metals. The synthetic method of two imino-phosphine frameworks was optimized, as well as the subsequent coordination reactions with first-row transition metals. The products were characterized utilizing a variety of spectroscopic techniques, including ^{1}H, ^{13}C, ^{31}P NMR and FT-IR spectroscopy, to confirm successful imine formation and metal complexation.

2,4,6-Triphenylaniline Imino-phosphine Ligand

The initial imino-phosphine framework was synthesized through a Schiff base condensation reaction utilizing 2-(diphenylphosphino)benzaldehyde and 2,4,6-triphenylaniline, as shown in Scheme. 1. This reaction was conducted on two different occasions on a large- and small-scale, with the large-scale batch utilizing 1.5 times the quantity of reagents, as shown in Table. 1. The resulting yield of the large-scale batch was substantially larger than the small-scale batch, 70.1 % and 58.0 % respectively. Following synthesis, the product of the large-scale procedure was characterized via ^{1}H, ^{13}C, ^{31}P NMR and FT-IR spectroscopy as discussed below.

Figure. 5 Picture of 2,4,6-triphenyaniline imino-phosphine ligand

The 500 MHz Bruker Spectrometer was able to produce ^{1}H spectral data, as shown in Table. 6 and Figure. 8, that confirmed the synthesis of the 2,4,6-triphenylaniline imino-phosphine ligand. Imine formation, which is the appearance of a carbon-nitrogen double bond, confirms a successful reaction between the aldehyde and amine in the Schiff base condensation reaction. Due to the proximation of the imine hydrogen to the electronegative nitrogen, this signal is produced further downfield than most hydrogens, at 8.9566 ppm. Interestingly, the imine hydrogen signal is demonstrated differently than expected, as a doublet rather than a singlet. It is predicted to present as a singlet due to the lack of hydrogens nearby, mitigating the imine hydrogen's ability to couple with other molecules. However, synthetic research on similar frameworks have reported this anomaly, and contributed the doublet to be a result of through-space coupling of the imine hydrogen to the phosphorus lone pair.[20,21] This theory was tested by employing ^{1}H $\{^{31}P\}$ NMR, effectively eliminating the possibility for coupling between the imine hydrogen and phosphorus.

As evidenced in Table. 9 and Figure. 11, the imine hydrogen signal is demonstrated as a singlet at 8.9607 ppm within this characterization, confirming previous suspicions that the imine hydrogen was performing through-space coupling to the phosphorus lone pair. Unfortunately, this compound cannot be considered pure due to ^{1}H spectral data indicating residual starting material. As shown within Table. 5 and Figure. 7, the spectral data for the starting material 2-(diphenylphosphino)benzaldehyde clearly demonstrate a singlet at 10.5137 ppm for the aldehyde hydrogen. An identical signal is demonstrated at 10.5340 ppm within the characterizations of 2,4,6-triphenylaniline imino-phosphine ligand, as shown in Table. 6 and Figure. 8. Therefore, this signal can be accredited to unreacted starting material present within the product.

Characterizations via ^{13}C $\{^{1}H\}$ and ^{31}P NMR spectroscopy allowed the investigation of further structural elucidation and coupling patterns within the 2,4,6-triphenylaniline imino-phosphine ligand. As shown in Table. 11 and Figure. 13, the ^{13}C $\{^{1}H\}$ spectral data present a phenomenon similar to that produced by the imine hydrogen, as the signal for the imine carbon is demonstrated by a doublet at 163.9418 ppm. The decoupling of the hydrogens within this characterization confirms that the carbon is not coupling to nearby hydrogens, however as evidenced by the doublet, the imine carbon is participating in coupling with another molecule. Similar to the imine hydrogen discussed previously, it can be theorized the imine carbon is engaging in through-space coupling to the phosphorus lone pair. In order to confirm this belief, future characterizations should be conducted via ^{13}C $\{^{31}P\}$ NMR spectroscopy. The ^{31}P spectral data in Table. 14 and Figure. 16 further demonstrate the presence of residual starting material, as demonstrated by the presence of a peak at -11.6297 ppm. As shown in Table. 13 and Figure. 15, the lone signal for the 2-(diphenylphosphino)benzaldehyde reagent is at -11.6314 ppm, similar placement to the peak within the ^{31}P spectra of the 2,4,6-triphenylaniline imino-phosphine ligand.

Condensation of the aldehyde to 2,4,6-triphenylaniline was also confirmed via FT-IR spectroscopy. The result of this characterization is presented in Table. 16 and Figure. 19, with the presence of an absorption band of medium strength at 1633.78 cm^{-1}, indicating the formation of a carbon-nitrogen double bond.[22]

4-Tritylaniline Imino-phoshine Ligand

The 4-tritylaniline imino-phosphine ligand was also synthesized via a Schiff base condensation reaction with 2-(diphenylphosphino)benzaldehyde; however, utilized a different amine from the previously mentioned imino-phosphine ligand, which was 4-tritylaniline. Initial synthesis of this compound demonstrated a crude sample with ample impurities, as a result, the reaction method, as shown in Scheme. 2, was optimized with the evaluation of various solvents for recrystallization. As evidenced in Table. 3, various trials were conducted to achieve purification of the 4-tritylaniline imino-phosphine ligand, with the combination amount of dichloromethane and methanol yielding the best results. The utilization of these solvents synthesized a product with 97.1 % yield and little impurities, as evident by the extensive characterizations conducted.

Figure. 6 Picture of 4-tritylaniline imino-phosphine ligand

This compound was characterized initially via a ^{1}H NMR spectrometer, with the spectral data recorded in Table. 7 and Figure. 9. As demonstrated by the imine hydrogen peak at 9.1616 ppm, formation of the expected product was successful. Similar to the 2,4,6-triphenylaniline imino-phosphine ligand, the imine hydrogen signal is demonstrated as a doublet, not the expected singlet. Following the same procedure to assess the coupling patterns within the 2,4,6-triphenylaniline imino-phosphine ligand, ^{1}H $\{^{31}P\}$ spectroscopy was conducted for the 4-tritylaniline imino-phosphine ligand. The result of this analysis is clearly shown in Table. 10 and Figure. 12, where it is confirmed the imine hydrogen within this compound is participating in a through-space coupling to the phosphorus lone pair.

Further characterizations via ^{13}C $\{^{1}H\}$, ^{31}P NMR and FT-IR spectroscopy indicated successful imine formation as well as the presentation of additional coupling patterns. The presence of a far downfield doublet at 163.9418 ppm within the ^{13}C $\{^{1}H\}$ spectrum, as shown in Table. 12 and Figure. 14, indicates condensation of the aldehyde to the aniline. As discussed previously for the 2,4,6-triphenylaniline imino-phosphine ligand, this signal is expected to be a singlet, and is proposed to be attributed to a through-space coupling between the imine carbon and the phosphorus lone pair. Further, the compounds ^{31}P spectral data, exhibited in Table. 15 and Figure. 17, indicates a sole peak at -13.6776 ppm, demonstrating the lone phosphorus atom within the 4-tritylaniline imino-phosphine ligand. Lastly, characterization via FT-IR

spectroscopy indicated an absorption band of medium strength at 1615.24 cm^{-1}, as shown in Table. 17 and Figure. 21, which is known to signify the presence of a carbon-nitrogen double bond.

^{1}H and ^{13}C NMR Spectra Comparison Between Imino-phosphine Ligands

The analysis of the signals for the imine carbons as well as phosphorus atoms between the imino-phosphine ligands present a curious shifting pattern. In regard to the ^{13}C spectral data, the imine carbon signal for the 2,4,6-triphenylaniline imino-phosphine ligand is further downfield than the signal from 4-tritylaniline imino-phosphine ligand, 163.9418 ppm and 158.5061 ppm respectively. The relative similarities of the two imino-phosphine ligand frameworks, as shown in Schemes. 1 and 2, indicate that the difference in signals may be due to possible resonance effects. Whilst comparing the structures, it is evident that the 2,4,6-triphenylaniline imino-phosphine ligand has more potential for resonance to shift electron density away from the 4-tritylaniline imino-phosphine ligand. As a result, this increased ability for resonance could shift the imine carbon of the 2,4,6-triphenylaniline imino-phosphine ligand further downfield as it is more deshielded than the 4-tritylaniline imino-phosphine ligand.

The shifting of the phosphorus atoms between the starting material, 2-DPPB, and the imino-phosphine ligands are also quite interesting. Unlike ^{1}H or ^{13}C NMR spectroscopy, phosphorus chemical shifts within ^{31}P NMR spectroscopy are not well understood, despite efforts of researchers worldwide.[23] Computational studies in recent decades have determined that chemical shifts within ^{31}P NMR spectroscopy rely on the paramagnetic shielding tensor, a calculation that depends on the energy of the excited states, radial expansion, which is the addition of new atoms at fixed angles and bond lengths, as well as bond overlap.[24] As a result, a trend within the chemical shifts shown in Figure. 18, where the phosphorus peak of 2-DPPB is the furthest downfield, followed by the 4-tritylaniline imino-phosphine ligand and finally the 2,4,6-triphenylaniline imino-phosphine ligand furthest upfield, is unable to be discerned at this time without further computational studies and analysis.

4-Tritylaniline Imino-Phosphine Ligand Coordinated to $CoCl_2$ or $ZnCl_2$

The previously synthesized 4-tritylaniline imino-phosphine ligand was coordinated to two different first-row transition metals, cobalt(II) chloride and zinc chloride. As demonstrated by Table. 4, the reaction utilizing $CoCl_2$ had a substantially higher yield than $ZnCl_2$, being 99.5

% and 58.4 % respectively. However, it is believed that the complexation product utilizing $CoCl_2$ had residual metal starting material that caused the increased percentage yield. This unreacted cobalt prevented the characterization of this coordinated product via NMR due to the impure, and heterogenous mixture. Alternatively, the complexation product utilizing $ZnCl_2$ was able to be characterized through ^1H NMR spectroscopy which confirmed successful complexation. As discussed previously, the imine hydrogen of both imino-phosphine ligand frameworks presented a doublet in ^1H NMR spectroscopy due to active through-space coupling to the phosphorus lone pair. Interestingly, once the 4-tritylaniline imino-phosphine ligand was complexed to $ZnCl_2$, the imine hydrogen signal was presented as a singlet, as shown in Table. 8 and Figure. 10. This change in coupling patterns can be attributed to the newly introduced metal cation, which is attached to the phosphorus atom and effectively preventing any possible coupling between the imine hydrogen and phosphorus lone pair.[20, 21] Additionally, an interesting trend was evident between the imino-phosphine ligand and its complexed product as the imine proton signals had an upfield shift. This phenomenon has been previously reported by various sources and is believed to be caused by the conformation change of the imino-phosphine ligand to allow for coordination to the metal centre.[20, 25, 26]

Future Work

This research presents significant progress for the development of a sustainable catalyst to be utilized in industrial hydroamination reactions. Continuing this synthetic research should firstly focus on product characterizations utilizing $^{13}C\ \{^{31}P\}$ and ^{31}P NMR spectroscopy. Further analysis via $^{13}C\ \{^{31}P\}$ NMR spectroscopy is required to elucidate the coupling patterns of the imine carbon, and the shifting patterns of the phosphorus atoms within the synthesized products can be analyzed via theoretical ^{31}P NMR spectroscopy. Additionally, future work on this project can focus on confirming coordination of the 4-tritylaniline imino-phosphine ligand with $CoCl_2$ through additional characterizations. To achieve this, optimizing the coordination method to ensure no residual $CoCl_2$ is left within the product would be a first step, as well as utilizing x-ray crystallography so as to confirm the expected structure. Moreover, further complexation studies utilizing the synthesized imino-phosphine ligand frameworks and additional first-row transition metals, such as iron and nickel, should be conducted. Developing and optimizing the coordination reactions with other first-row transition metals will allow for increased variety of the catalysts synthesized, as well as allow for the determination of the most suitable candidates for industrial alternatives. Finally, a vital component within this research is to assess the catalytic efficiency of the synthesized products by utilizing them within hydroamination reactions. Unfortunately, this aspect of the research was not able to be completed but is integral to the viability of these catalysts for future industrial alternatives.

Conclusion

This project successfully developed a catalyst for industrial hydroamination reactions utilizing an imino-phosphine ligand framework and readily available first-row transition metals. Two novel imino-phosphine ligands were synthesized, utilizing 2,4,6-triphenylaniline and 4-tritylaniline, with a 70.1 % and 97.0 % yield respectively. Characterizations of the imino-phosphine ligands via ^{1}H, ^{13}C, ^{31}P NMR and FT-IR spectroscopy confirmed imine formation, and coordination of $ZnCl_2$ to the 4-tritylaniline imino-phosphine ligand was confirmed via ^{1}H NMR spectroscopy.

References

1. Streiff, S.; Jérôme, F. *Chem. Soc. Rev.*, **2021**, *50*, 1512-1521.
2. Pohlki, F.; Doye, S. *Chem. Soc. Rev.*, **2003**, *32*, 104-114.
3. Müller, T.; Hultzsch, K. C.; Yus, M.; Foubelo, F.; Tada, M. *Chem. Rev.* **2008,** *108*, 3795-3892.
4. Ackermann, L.; Bergman, R. G.; Loy, R. N. *J. Am. Chem. Soc*. **2003**, *125*, 11956-11963.
5. Yim, J. C.; Schager, L. L. *EurJOC*. **2014**, *31*, 6825-6840.
6. Ludwig, J. R.; Schindler, C. S. *Chem.* **2017**, *2*, 313-316.
7. American Chemical Society. 12 Principles of Green Chemistry. https://www.acs.org/greenchemistry/principles/12-principles-of-green-chemistry.html (Accessed March 20, 2023)
8. Müller, T. E.; Beller, M. *Chem. Rev.* **1998**, *98*, 675-704.
9. Hong, S.; Marks, T. J. *Acc. Chem. Res.* **2004**, *37*, 673-686.
10. Ohmiya, H.; Moriya, T.; Sawamura, M. *Org. Lett.* **2009**, *11*, 2145-2147.
11. Taylor, J. G., Whittal, N., Kuock, K. Hii, M. *Org. Lett.* **2006**, *8*, 3561 – 3564.
12. Komeyama, K., Morimoto, T., Takaki, K. *Angew. Chem.* **2006**, *45*, 2938 – 2941.
13. Senn, H. M.; Blöchl, P. E.; Togni, A. *J. Am. Chem. Soc.* **2000,** *122*, 4009-4107.
14. LibreTexts Chemistry. Hydroamination Reactions of Alkenes. https://chem.libretexts.org/Bookshelves/Organic_Chemistry/Supplemental_Modules_(Organic_Chemistry)/Reactions/Organic_Reactions/Hydroamination_Reactions_of_Alkenes (Accessed March 20, 2023)
15. Nguyen, T. M., Nicewicz, D. A. *J. Am. Chem. Soc.* **2012,** *135*, 9588 – 9591.
16. Utsunomiya, M.; Kuwano, R.; Kawatura, M.; Hartwig. J. F. *J. Am. Chem. Soc.* **2004,** *123*, 5608-5609.
17. Colonna, P., Bexxenine, S., Gil, R., Hannedouche, J. *Adv. Synth. Catal.* **2020**, *362*, 1550-1563.
18. Zhao, J., Goldman, A. S., Hartwig, J. F. *Science*, **2005**, *307*, 1080-1082.
19. Khaskin, E., Iron, M. A., Shimon, J. W., Zhang, J., Milstein, D. *J. Am. Chem. Soc.* 2010, *132*, 8542-8543
20. Mogorosi, M. M., Mahamo, T., Moss, J. R., Mapolie, S. F., Slootweg, J. C., Lammertsma, K., Smith, G. S. *J. Organomet. Chem.* **2011,** *696*, 3585-3592.

21. Motswainhana, W. M., Onani, M. O., Madiehe, A. M., Saibu, M., Thovhogi, N., Lalancette, R. A. *J. Inorg. Biochem.* **2013**, *129*, 112-118.
22. Millipore Sigma. IR Spectrum Table and Chart. https://www.sigmaaldrich.com/CA/en/technical-documents/technical-article/analytical-chemistry/photometry-and-reflectometry/ir-spectrum-table (Accessed April 3, 2023)
23. Feindel, K. W., Wasylishen, R. E., *Can. J. Chem.* **2011,** *82*, 27 – 44.
24. Wikipedia. Phosphorus-31 Nuclear Magnetic Resonance. https://en.wikipedia.org/wiki/Phosphorus-31_nuclear_magnetic_resonance (Accessed April 7, 2023)
25. Motswainyana, W. M., Ojwach, S. O., Onani, M. O., Iwuoha, E., Darkwa, J. *Polyhedron.* **2011,** *30, 2574-2580.*
26. Reddy, K. R., Surekha, K., Lee, G., Peng, S., Chen, J., Liu, S. *Organometallics.* **2001**, *20*, 1292 – 1299.

Appendix

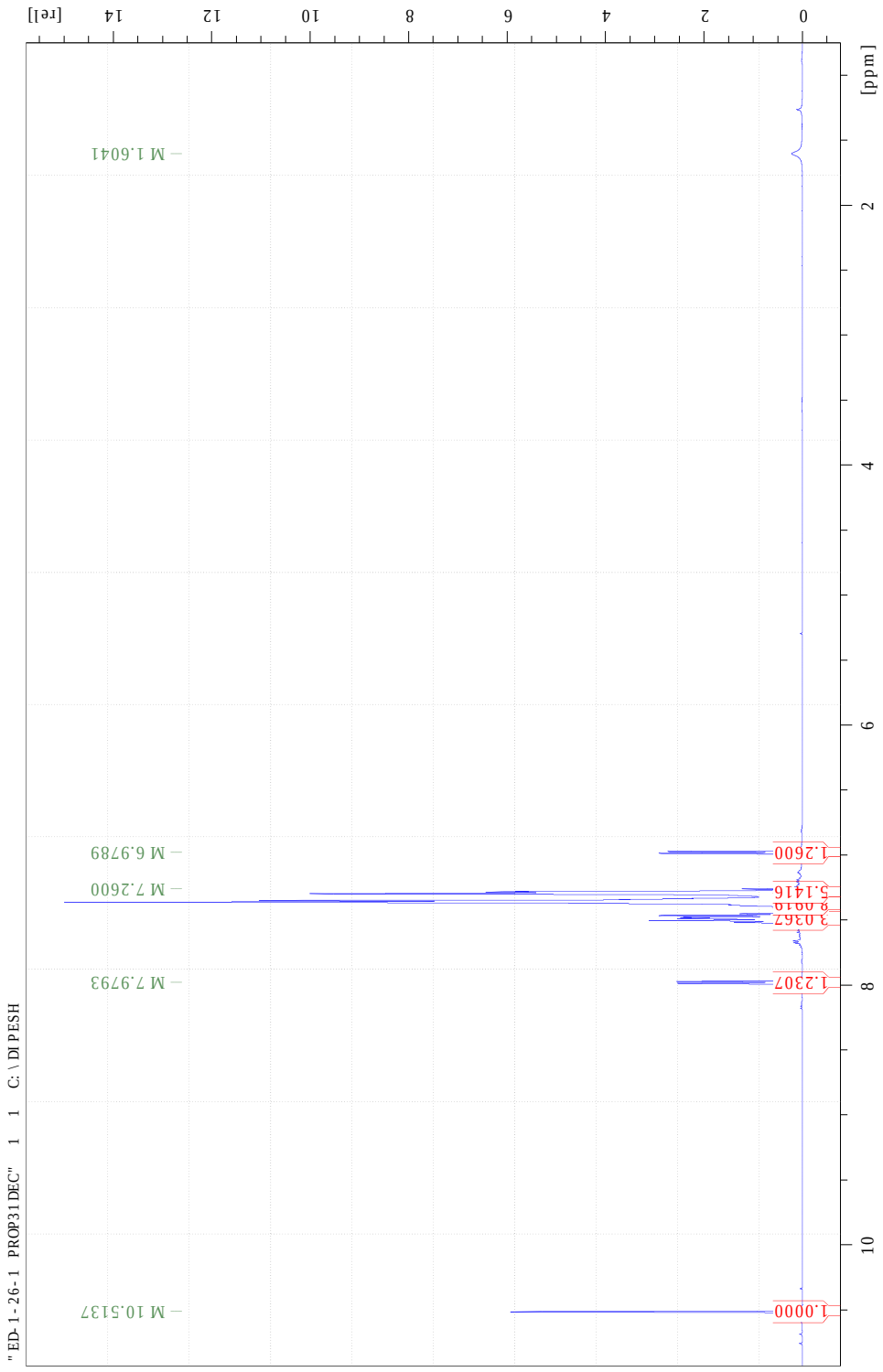

Figure. 7 ^{1}H NMR of 2-(diphenylphosphino)benzaldehyde

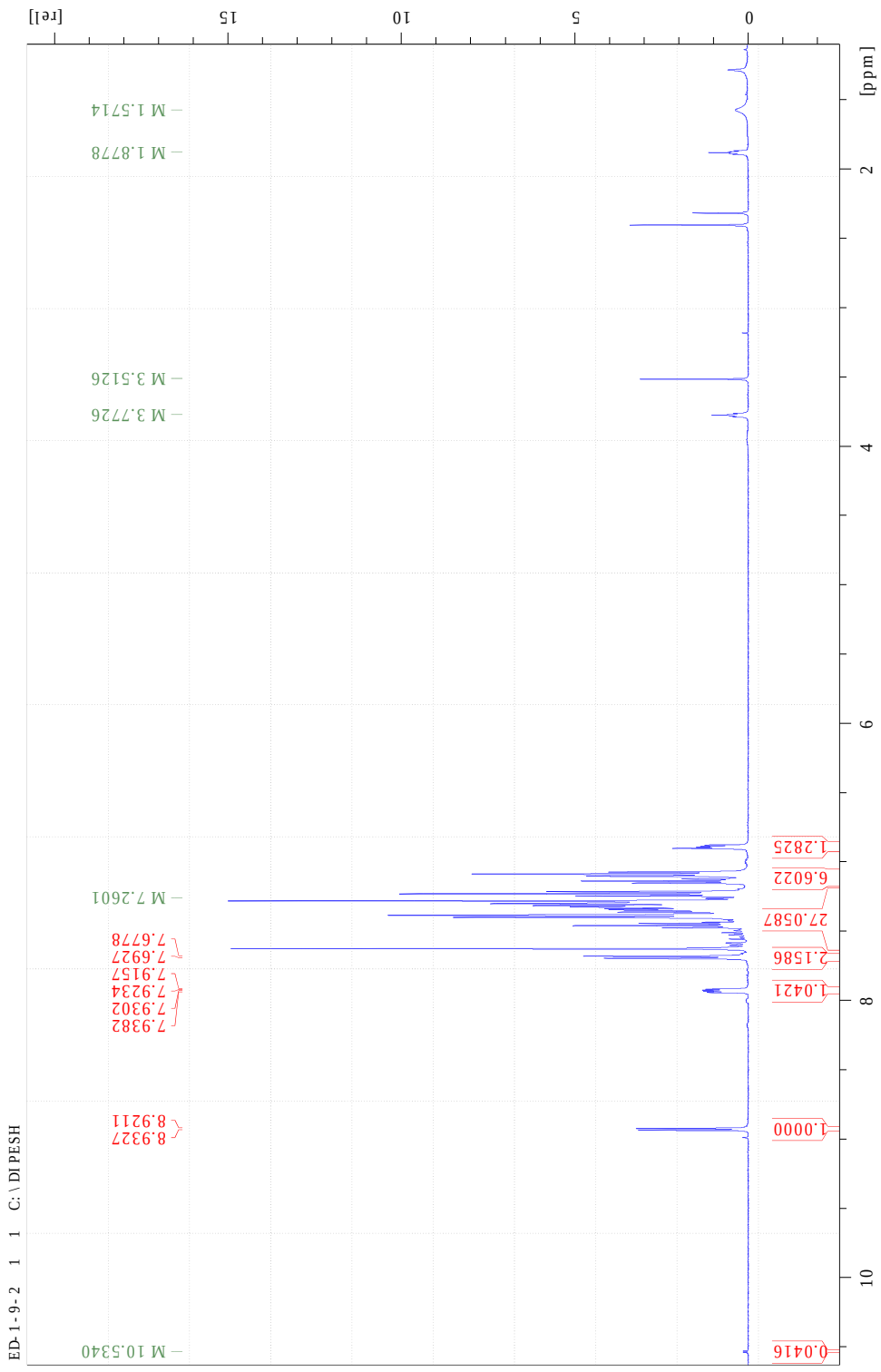

Figure. 8 ^{1}H NMR of the 2,4,6-triphenylaniline imino-phosphine ligand

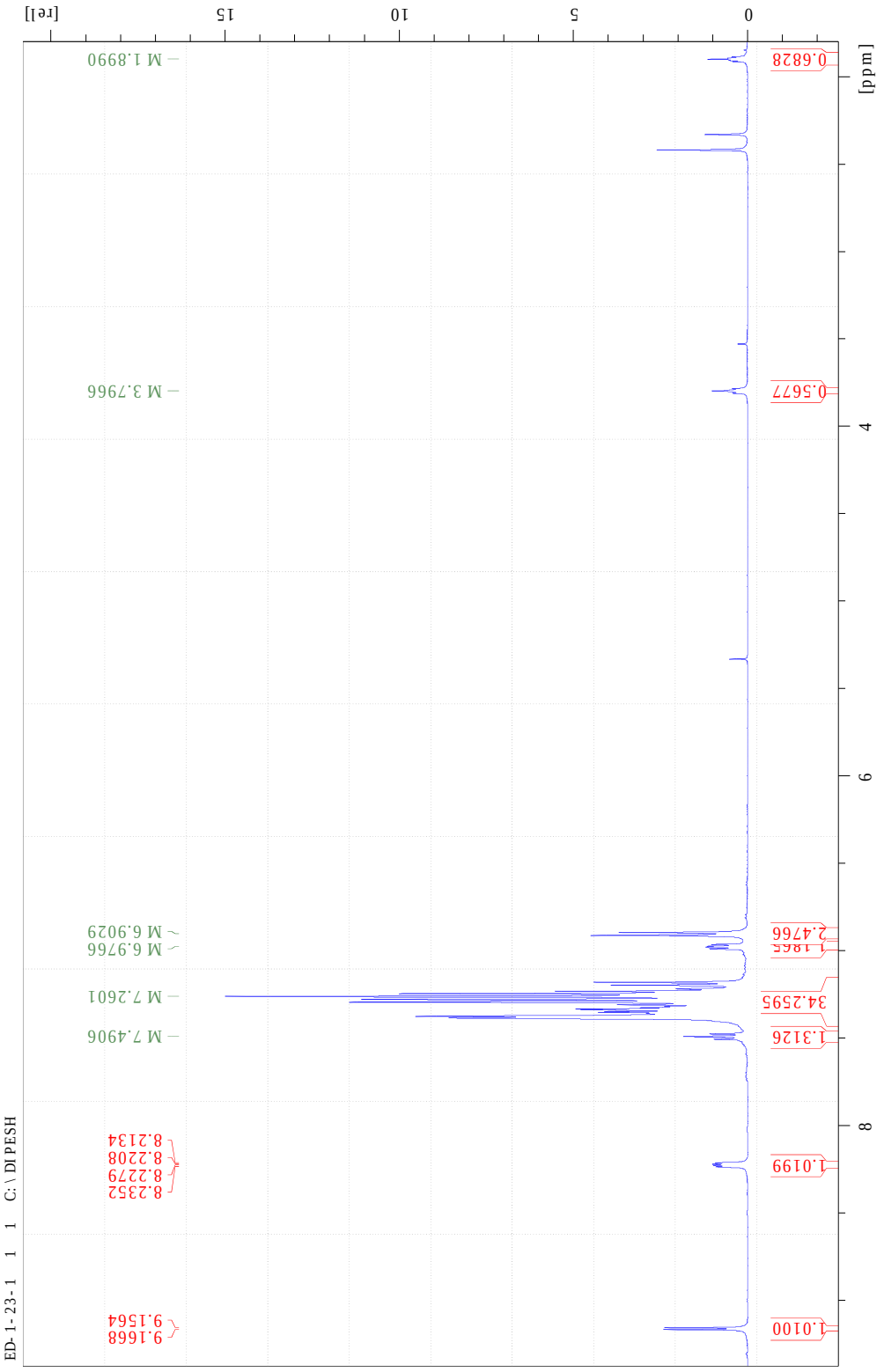

Figure. 9 ^{1}H NMR of the 4-tritylaniline imino-phosphine ligand

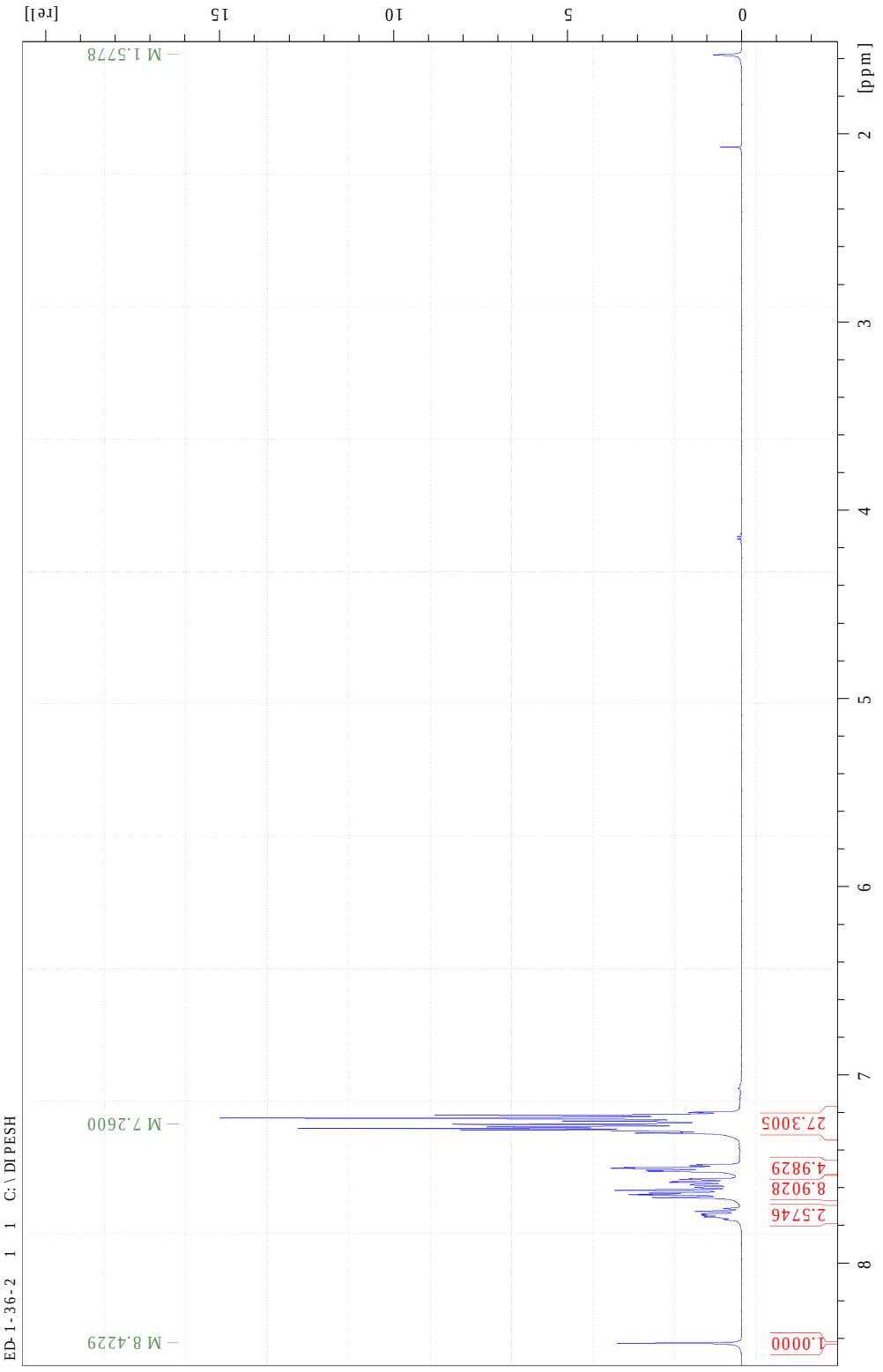

Figure. 10 ^{1}H NMR of the 4-tritylaniline imino-phosphine ligand complexed to $ZnCl_2$

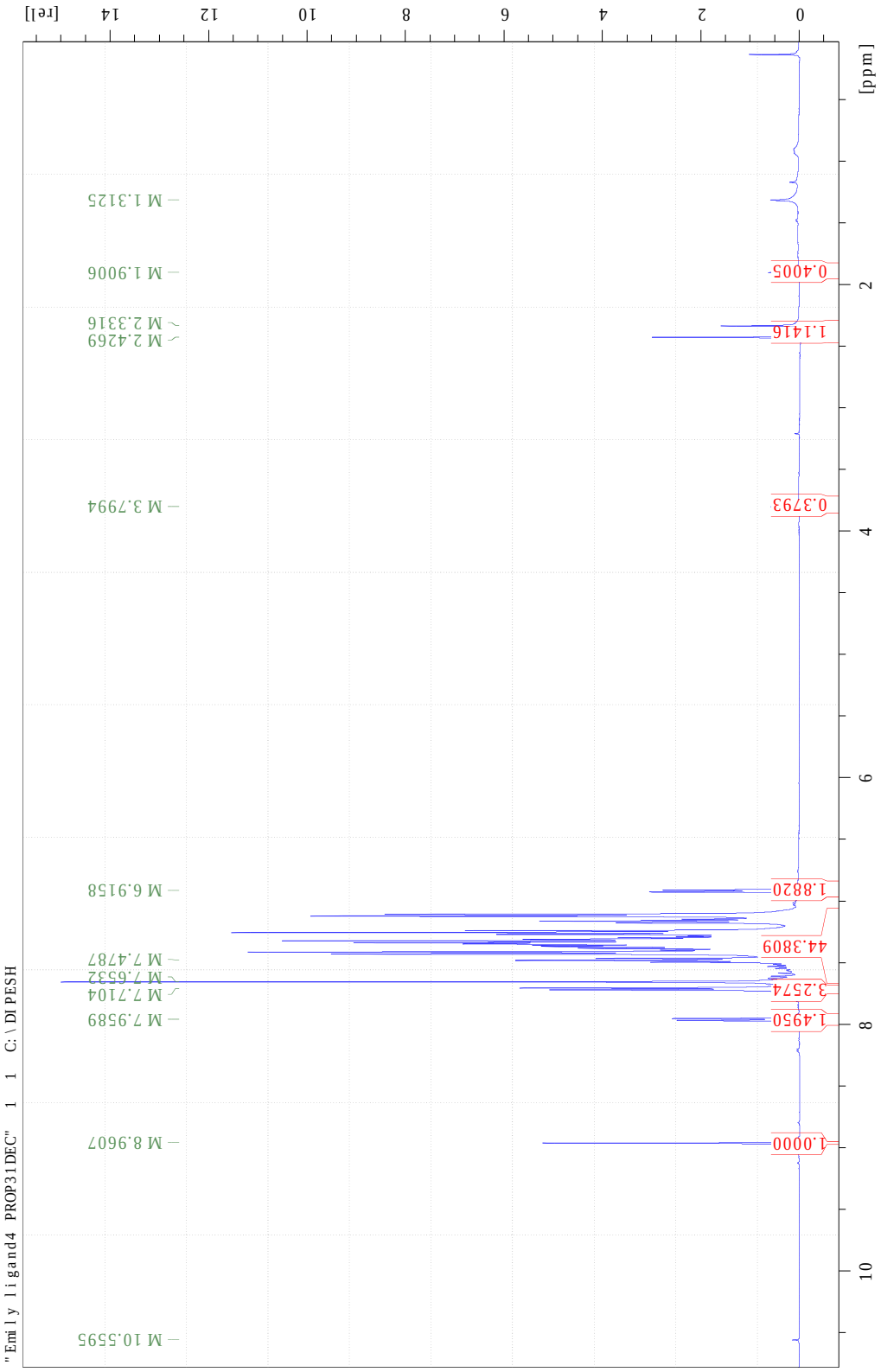

Figure. 11 ^{1}H NMR with ^{31}P decoupled of the 2,4,6-triphenylaniline imino-phosphine ligand

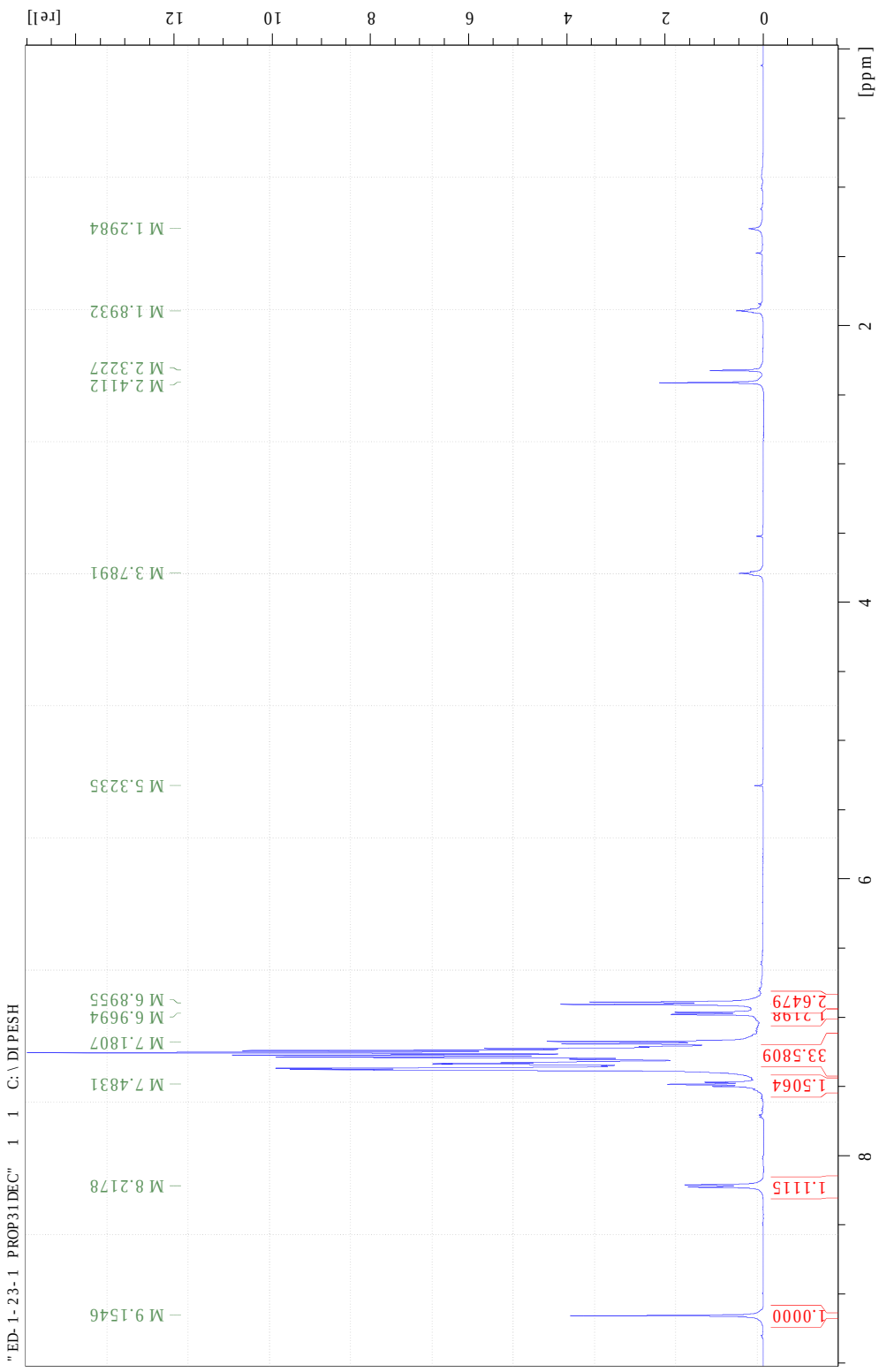

Figure. 12 ^{1}H NMR with ^{31}P decoupled of the 4-tritylaniline imino-phosphine ligand

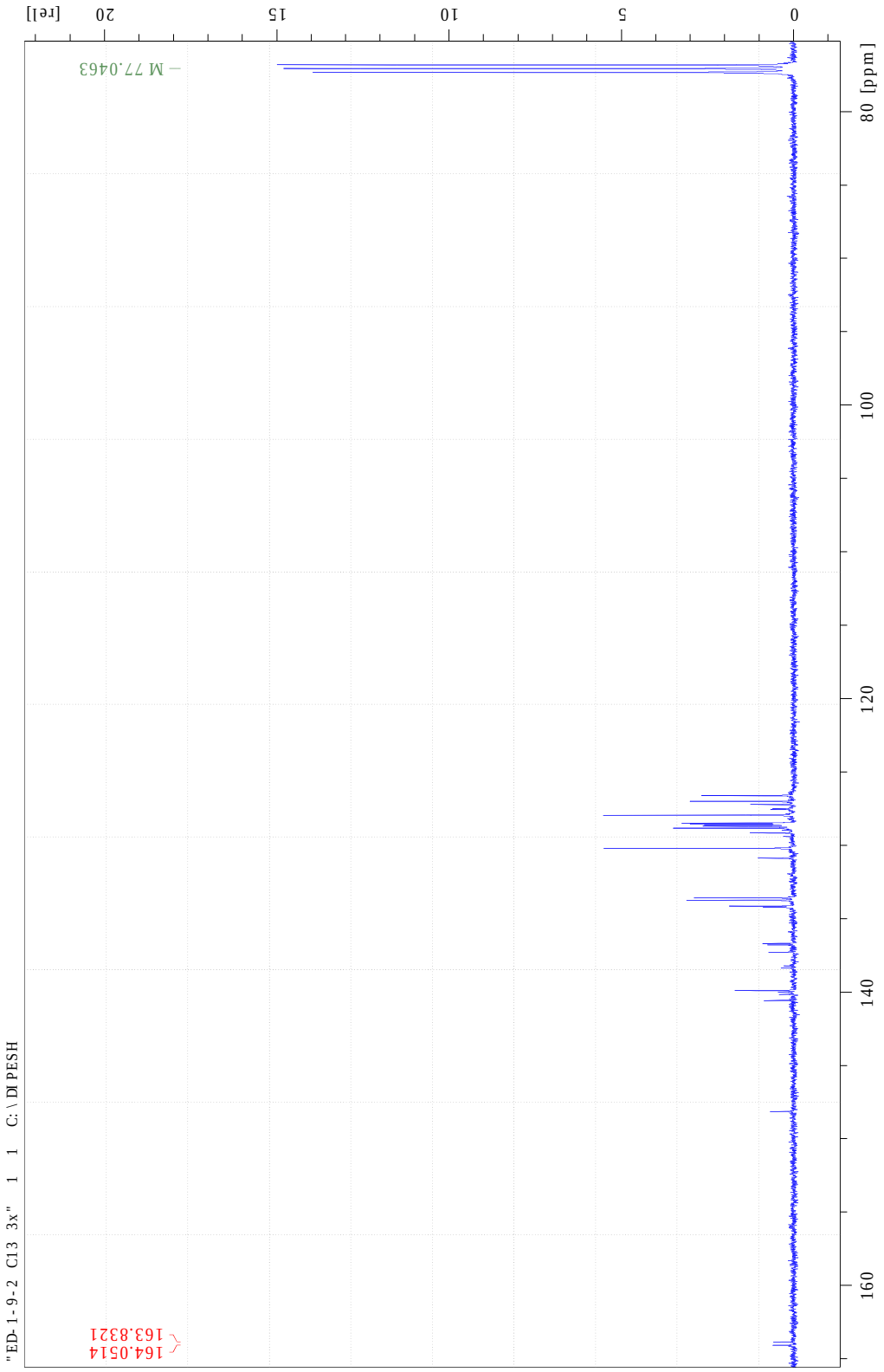

Figure. 13 ^{13}C NMR of the 2,4,6-triphenylaniline imino-phosphine ligand

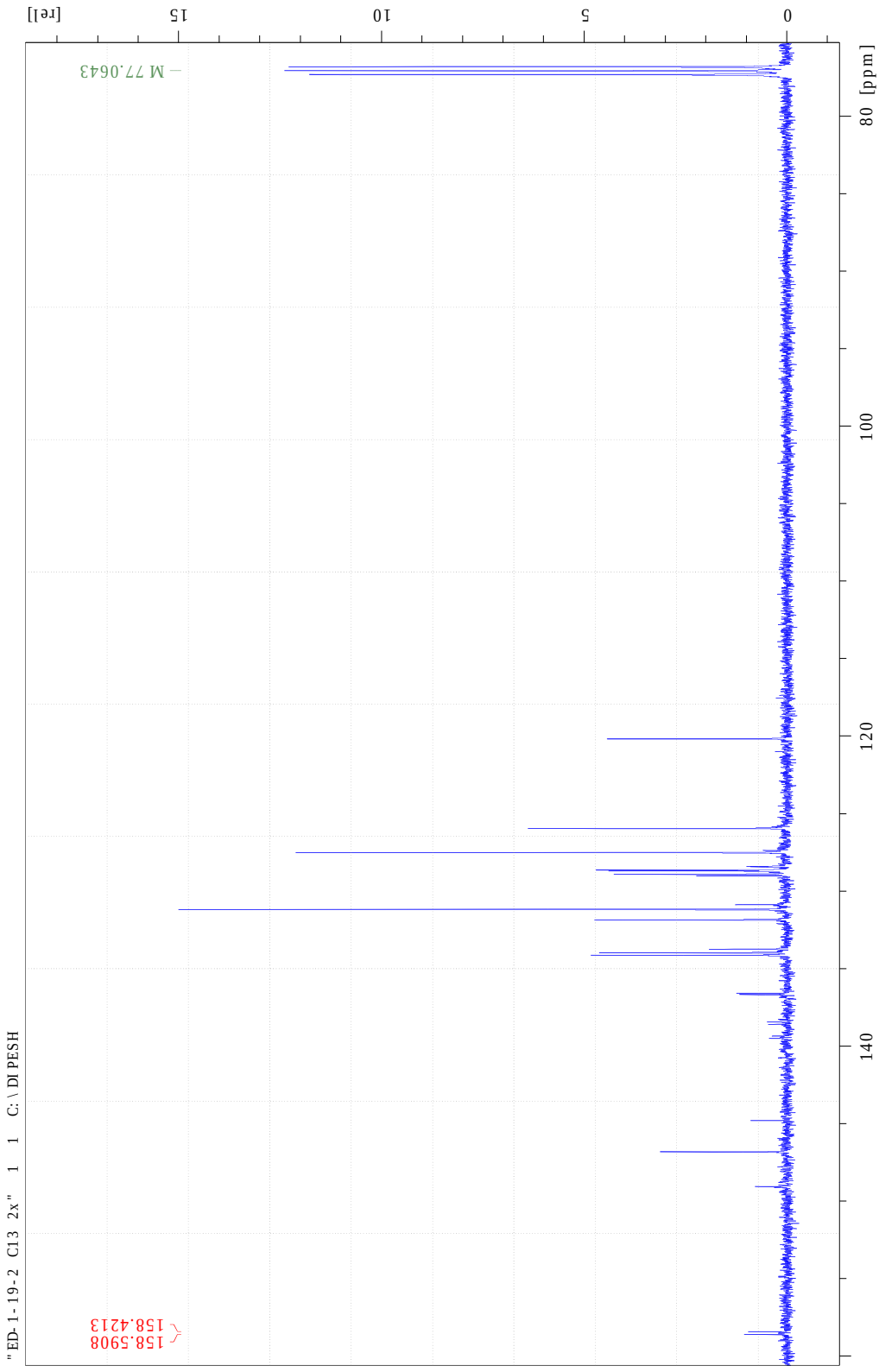

Figure. 14 ^{13}C of the 4-tritylaniline imino-phosphine ligand

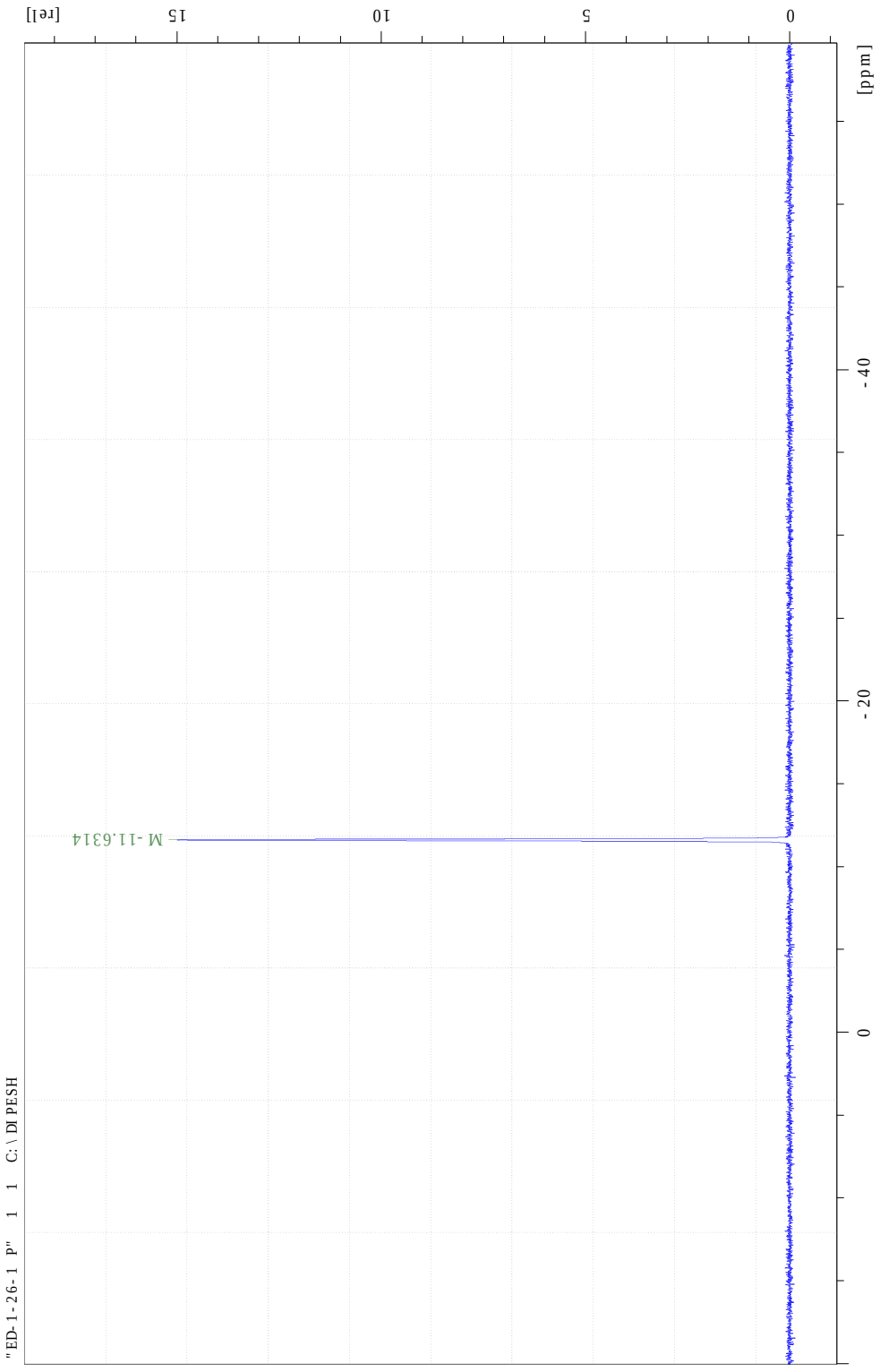

Figure. 15 ^{31}P NMR of 2-(diphenylphosphino)benzandaldehyde

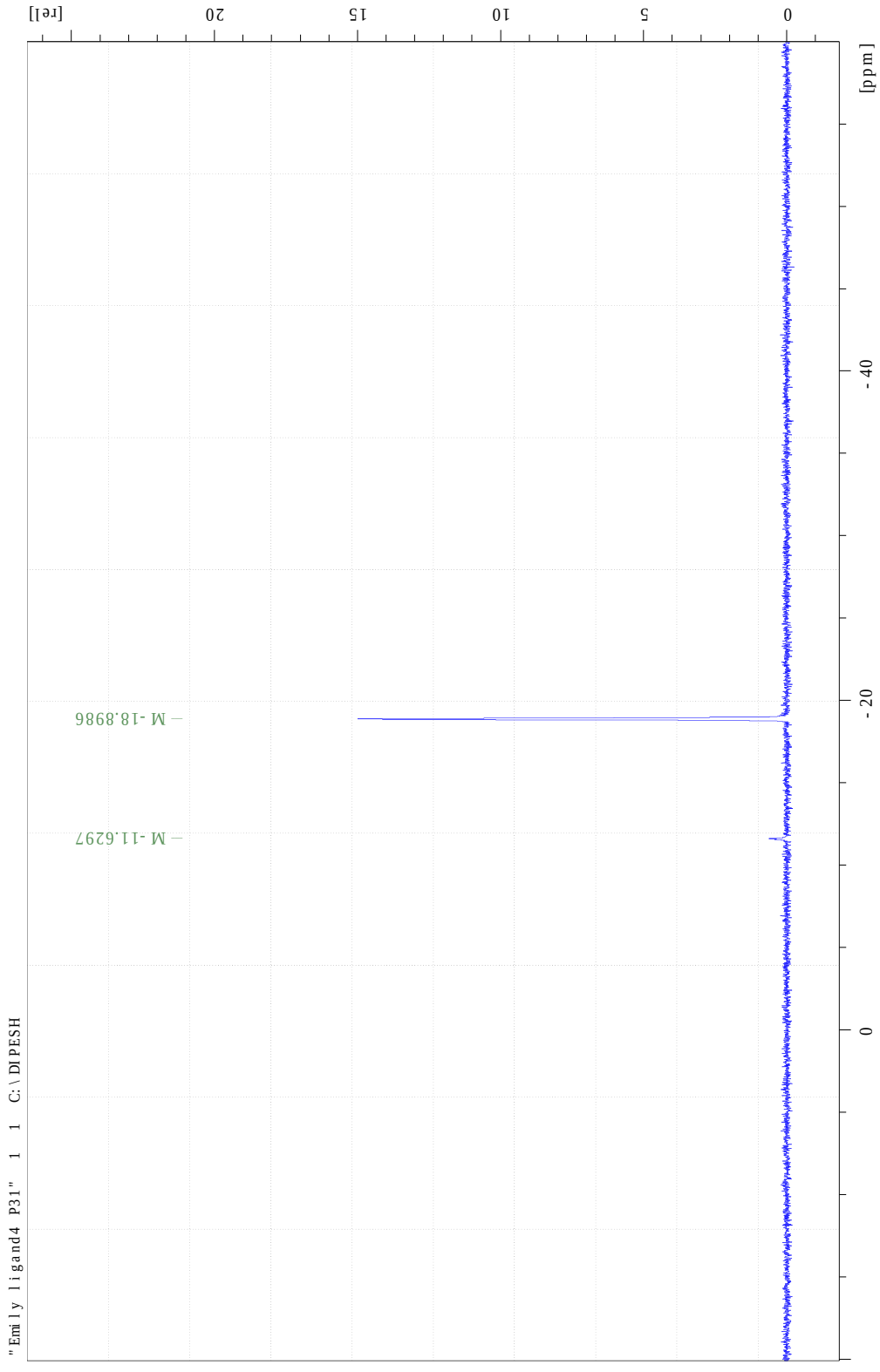

Figure. 16 ^{31}P NMR of the 2,4,6-triphenylaniline imino-phosphine ligand

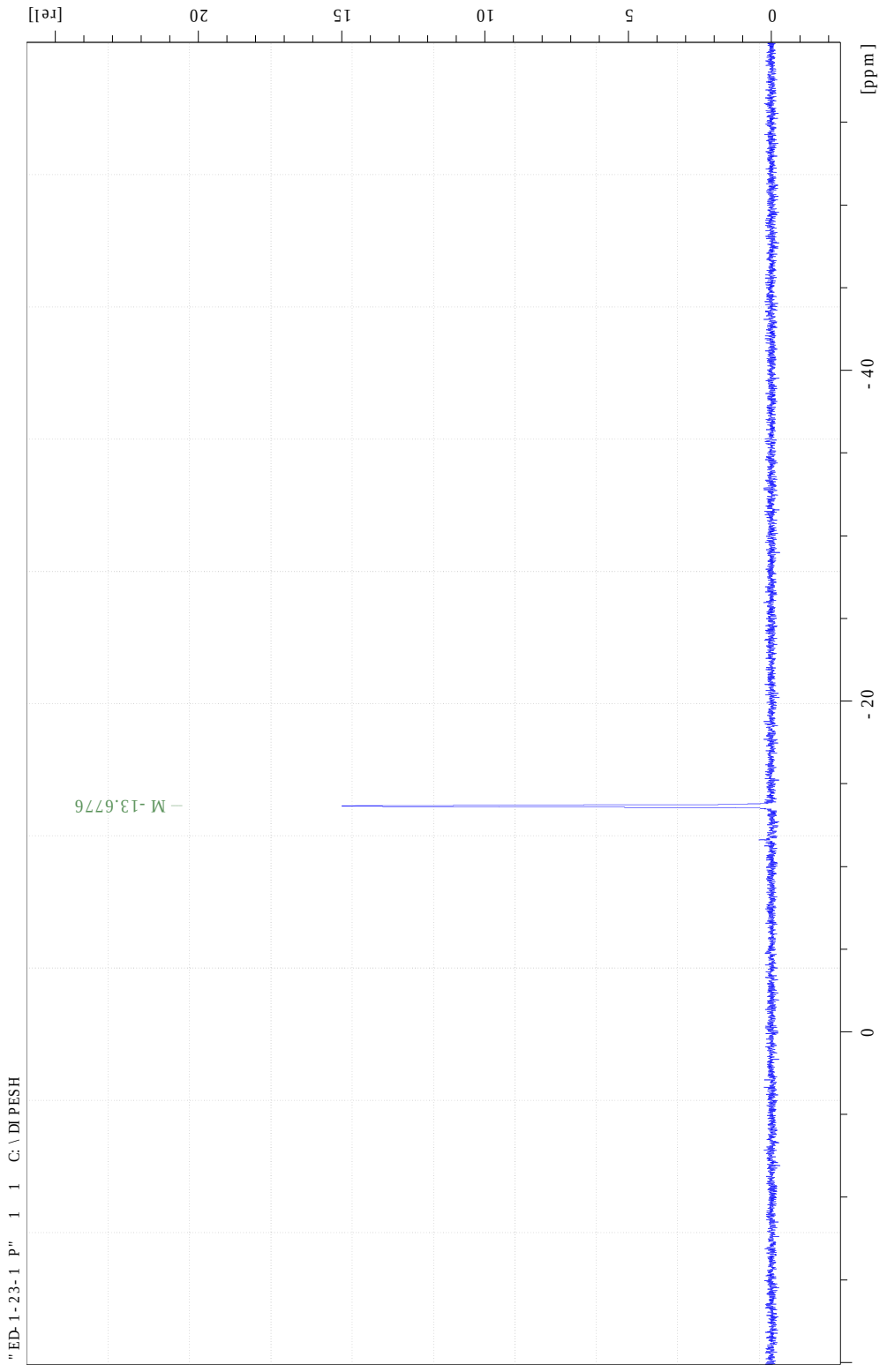

Figure. 17 ^{31}P NMR of the 4-tritylaniline imino-phosphine ligand

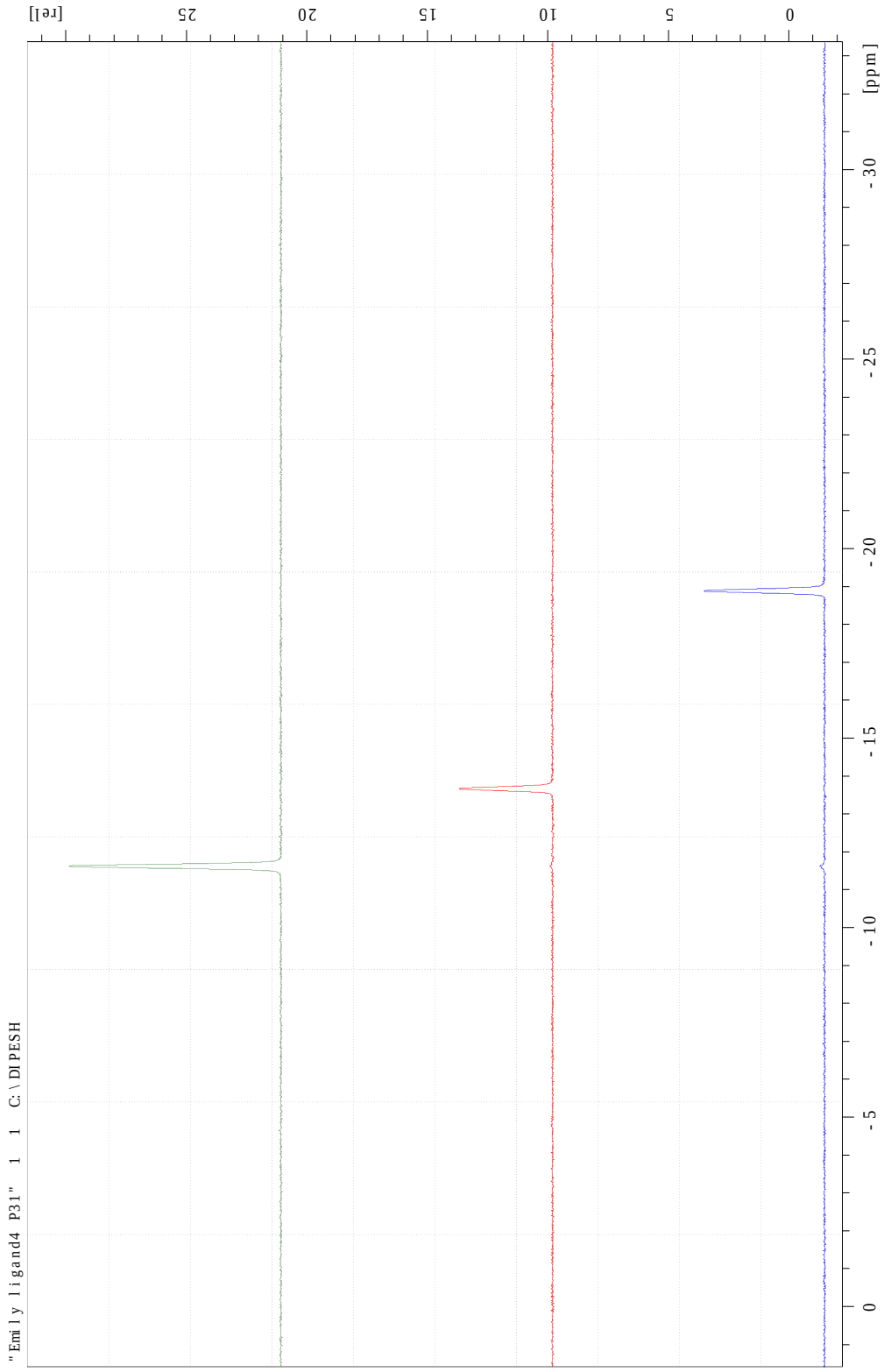

Figure. 18 ^{31}P NMR of 2-(diphenylphosphino)benzaldehyde (Top), 2,4,6-triphenylaniline imino-phosphine ligand (Middle), 4-tritylaniline imino-phosphine ligand (Bottom)

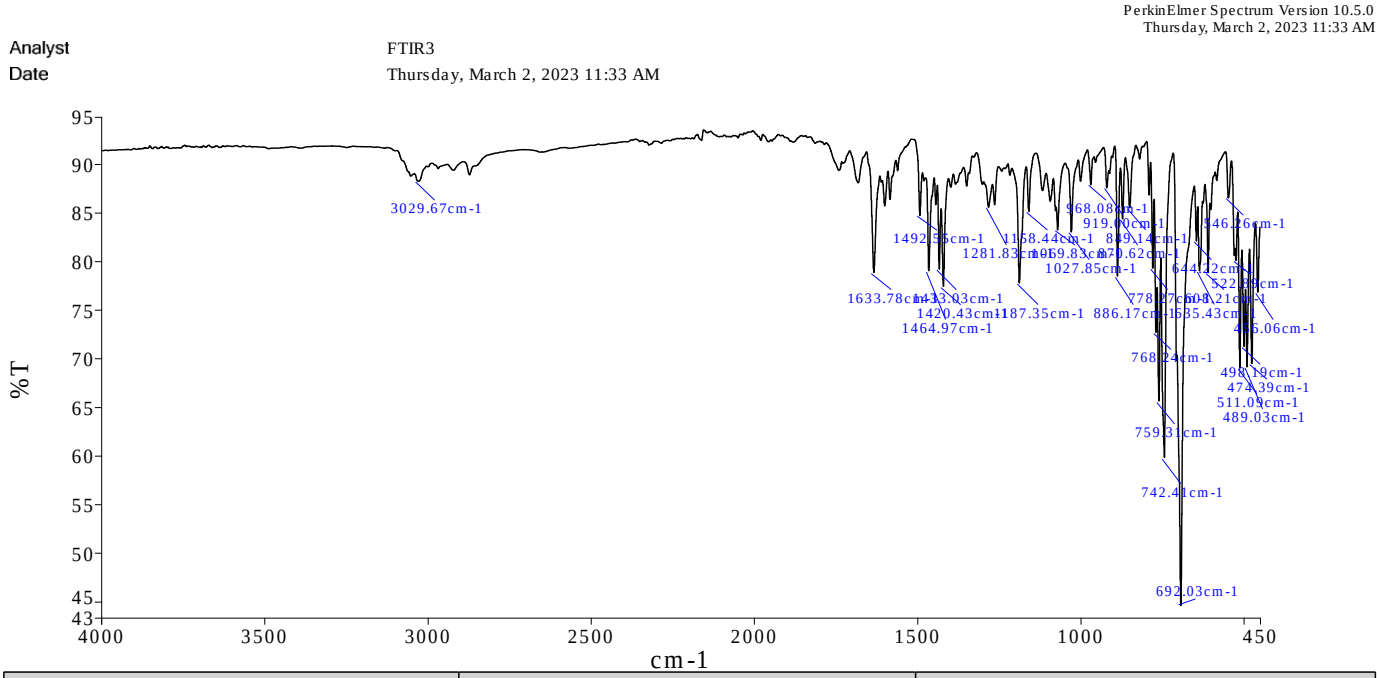

Sample Name	Description	Quality Checks
ED-1-9-2	Sample 476 By FTIR3 Date Thursday, March 02 2023	The Quality Checks do not report any warnings for the sample.

Figure. 19 FT-IR spectra of 2,4,6-triphenylaniline imino-phosphine ligand

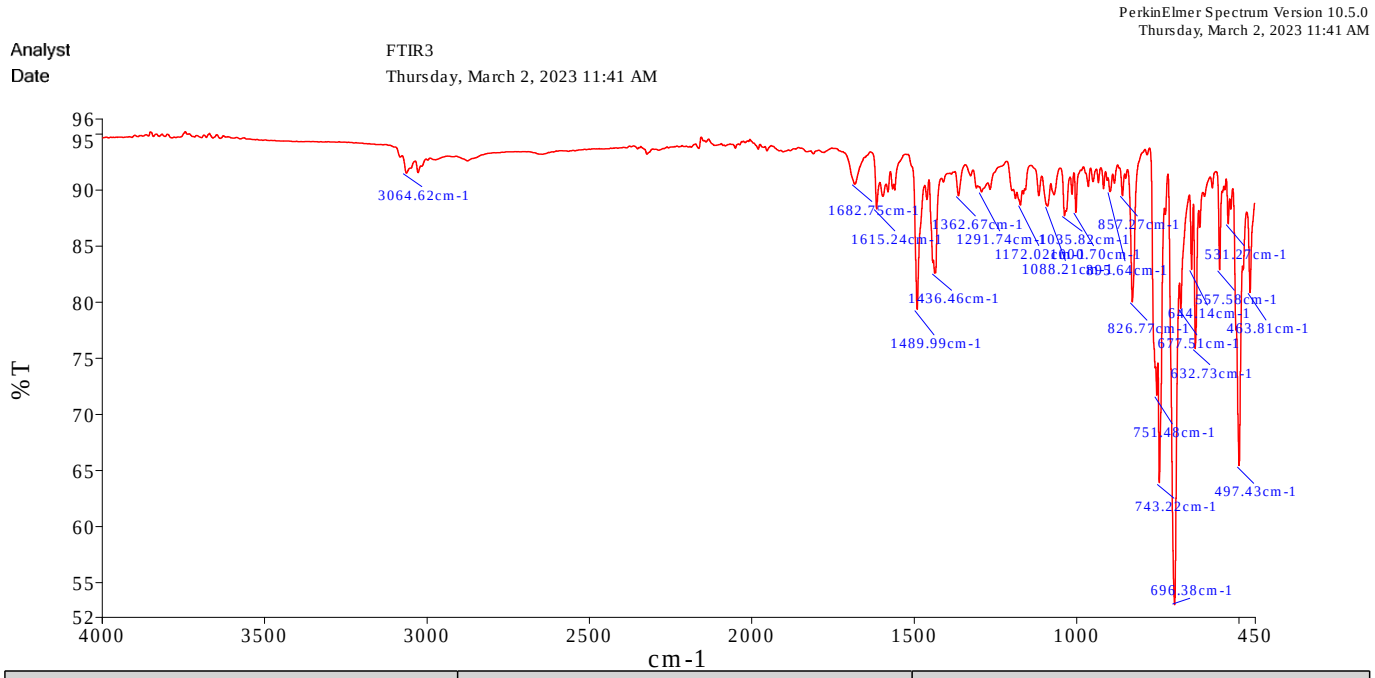

Sample Name	Description	Quality Checks
ED-1-19-2	Sample 477 By FTIR3 Date Thursday, March 02 2023	The Quality Checks do not report any warnings for the sample.

Figure. 20 FT-IR spectra of 4-tritylaniline imino-phosphine ligand